

LETTER TO THE EDITOR

Discovery of allenyl acetylene, H₂CCCHCCH, in TMC-1. A study of the isomers of C₅H₄ [★]

J. Cernicharo¹, C. Cabezas¹, M. Agúndez¹, B. Tercero^{2,3}, N. Marcelino¹, J. R. Pardo¹, F. Tercero², J.D. Gallego², J.A. López-Pérez², P. deVicente²

¹ Grupo de Astrofísica Molecular, Instituto de Física Fundamental (IFF-CSIC), C/ Serrano 121, 28006 Madrid, Spain. e-mail: jose.cernicharo@csic.es

² Centro de Desarrollos Tecnológicos, Observatorio de Yebes (IGN), 19141 Yebes, Guadalajara, Spain.

³ Observatorio Astronómico Nacional (OAN, IGN), Madrid, Spain.

Received; accepted

ABSTRACT

We present the discovery in TMC-1 of allenyl acetylene, H₂CCCHCCH, through the observation of nineteen lines with a signal-to-noise ratio ~4-15. For this species, we derived a rotational temperature of 7±1K and a column density of 1.2±0.2×10¹³ cm⁻². The other well known isomer of this molecule, methyl diacetylene (CH₃C₄H), has also been observed and we derived a similar rotational temperature, T_r=7.0±0.3 K, and a column density for its two states (*A* and *E*) of 6.5±0.3×10¹² cm⁻². Hence, allenyl acetylene and methyl diacetylene have a similar abundance. Remarkably, their abundances are close to that of vinyl acetylene (CH₂CHCCH). We also searched for the other isomer of C₅H₄, HCCCH₂CCH (1.4-Pentadiyne), but only a 3σ upper limit of 2.5×10¹² cm⁻² to the column density can be established. These results have been compared to state-of-the-art chemical models for TMC-1, indicating the important role of these hydrocarbons in its chemistry.

The rotational parameters of allenyl acetylene have been improved by fitting the existing laboratory data together with the frequencies of the transitions observed in TMC-1.

Key words. molecular data — line: identification — ISM: molecules — ISM: individual (TMC-1) — astrochemistry

1. Introduction

More than 200 different chemical species have been detected in space. Most of them have a large dipole moment which permits an easy search for their rotational transitions through radio astronomical observations. However, only a few pure hydrocarbons, C_nH_m (with m≥2), have been detected so far, and their role in the chemistry of cold dark clouds is poorly understood. Molecules such as C₂H₂, C₂H₄, and C₂H₆, which lack a permanent dipole moment, are studied through their derivatives, mainly through the replacement of a hydrogen atom by the CN radical. In this context, it is worth noting that while CH₂CHCN was detected in the early years of millimeter radio astronomy, its equivalent with the CCH group, vinyl acetylene, has been detected only recently towards the cold dark cloud TMC-1 with an abundance that is twice that of the cyanide derivative (Cernicharo et al. 2021a). This is mainly due to the huge difference in the dipole moments of CH₂CHCN (μ_a=3.821 D, Kraśnicki & Kisiel 2011) and CH₂CHCCH (μ_a=0.43 D, Sobolev et al. 1962). Hence, only a few hydrocarbons with a low dipole moment have been found so far in the interstellar medium (ISM). Among them are propene (Marcelino et al. 2007), with a dipole moment of 0.36 D (Lide & Mann 1957), and deuterated methane, which has been tentatively detected towards the low mass protostar IRAS 04368+2557 (Sakai et al. 2012). The later species has a

very low dipole moment indeed, 0.0056 D (Ozier et al. 1969). Pure unsaturated hydrocarbons radicals, C_nH, and their anions, have moderate to very large dipole moments and have been detected up to n = 8 in interstellar and circumstellar clouds (Cernicharo & Guélin 1996; Remijan et al. 2007; Kawaguchi et al. 2007).

In this letter, we report on the discovery of allenyl acetylene, H₂CCCHCCH (also named ethynyl allene), through nineteen well detected rotational transitions. This species was spectroscopically characterised (McCarthy et al. 2020), but never detected in space. It is one of the possible isomers with molecular formula C₅H₄. We compare the derived abundance with that of other acetylenic species such as CH₃C₄H (another C₅H₄ isomer), CH₃CCH, and CH₂CHCCH (the two latter species are C₄H₄ isomers). We also searched for another C₅H₄ isomer, HCCCH₂CCH, but only upper limits are obtained. These results are analysed in the context of a state-of-the-art chemical model of a cold dark cloud.

2. Observations

New receivers, which were built within the Nanocosmos project¹ and installed at the Yebes 40m radiotelescope, were used for the observations of TMC-1. The Q-band receiver consists of two high electron mobility transistor cold amplifiers, covering the 31.0-50.3 GHz range with horizontal and vertical polarisations. Receiver temperatures vary from 22 K at 32 GHz to 42 K at

[★] Based on observations carried out with the Yebes 40m telescope (projects 19A003, 19A010, 20A014, 20D023). The 40m radiotelescope at Yebes Observatory is operated by the Spanish Geographic Institute (IGN, Ministerio de Transportes, Movilidad y Agenda Urbana).

¹ <https://nanocosmos.iff.csic.es/>

50 GHz. Eight 2.5 GHz wide fast Fourier transform spectrometers (FFTs), with a spectral resolution of 38.15 kHz, provide the whole coverage of the Q-band in each polarization. The main beam efficiency varies from 0.6 at 32 GHz to 0.43 at 50 GHz. A detailed description of the system is given by Tercero et al. (2020).

The line survey of TMC-1 ($\alpha_{J2000} = 4^{\text{h}}41^{\text{m}}41.9^{\text{s}}$ and $\delta_{J2000} = +25^{\circ}41'27.0''$) in the Q-band was performed in several sessions. Previous results for the detection of C_3N^- and C_5N^- (Cernicharo et al. 2020b), HC_5NH^+ (Marcelino et al. 2020), HC_4NC (Cernicharo et al. 2020c), and HC_3O^+ (Cernicharo et al. 2020a) were based on two observing runs performed in November 2019 and February 2020. Two different frequency coverages were achieved, 31.08-49.52 GHz and 31.98-50.42 GHz, in order to check that no spurious spectral ghosts were produced in the down-conversion chain, which downconverts the signal from the receiver to 1-19.5 GHz and then splits it into 8 2.5 GHz bands which are finally analysed by the FFTs. Additional data were taken in October and December 2020. A final observing run was performed in January 2021 to improve the line survey and to further check the consistency of all observed spectral features. These new data have allowed the detection of HC_3S^+ (Cernicharo et al. 2021b) along with the acetyl cation, CH_3CO^+ (Cernicharo et al. 2020c), HDCCN (Cabezas et al. 2021), the isomers of $\text{C}_4\text{H}_3\text{N}$ (Marcelino et al. 2021), and vinyl acetylene (Cernicharo et al. 2021a).

The observations were carried out using frequency switching with a frequency throw of 10 MHz for the first two runs and of 8 MHz for the later ones. The intensity scale, antenna temperature (T_A^*), was calibrated using two absorbers at different temperatures and the atmospheric transmission model (ATM; Cernicharo 1985; Pardo et al. 2001). Calibration uncertainties have been adopted to be 10 %. The nominal spectral resolution of 38.15 kHz was used for the final spectra. The sensitivity varies across the Q-band from 0.3 to 2.0 mK. All data have been analysed using the GILDAS package².

3. Results and discussion

The sensitivity of our observations towards TMC-1 (see section 2) is a factor of 10-20 better than in previously published line surveys of this source at the same frequencies (Kaifu et al. 2004). This large improvement has allowed us to detect a forest of weak lines. In fact, it has been possible to detect many individual lines (Marcelino et al. 2021) from molecular species that were reported previously only by stacking techniques (Marcelino et al. 2021). Taking into account the large abundance found in TMC-1 for cyanide derivatives of abundant species, and of the presence of nearly saturated hydrocarbons, such as CH_3CHCH_2 (Marcelino et al. 2007) and CH_2CHCCH (Cernicharo et al. 2021a), we searched for similar species containing CCH such as $\text{H}_2\text{CCCHCCH}$ and HCCCH_2CCH . We compared the derived abundances with that of the well know species in this source methyl diacetylene, $\text{CH}_3\text{C}_4\text{H}$ (MacLeod et al. 1984; Walmsley et al. 1984). Line identifications in this TMC-1 survey were performed using the MADEX catalogue (Cernicharo 2012), the Cologne Database of Molecular Spectroscopy catalogue (CDMS; Müller et al. 2005), and the JPL catalogue (Pickett et al. 1998).

3.1. Allenyl acetylene, $\text{H}_2\text{CCCHCCH}$

Allenyl acetylene is one of the possible C_5H_4 isomers. We calculated the relative energies of its three most stable isomers, namely $\text{H}_2\text{CCCHCCH}$, $\text{CH}_3\text{C}_4\text{H}$, and HCCCH_2CCH . Structural optimisation calculations for the lowest energy conformers of each isomer were done using the Møller-Plesset post-Hartree-Fock method (Møller & Plesset 1934) and explicitly electron correlation effects through perturbation theory up to the second and the Dunning's consistent polarised valence triple- ζ basis set (MP2/cc-pVTZ) (Dunning 1989). These calculations were performed using the Gaussian 09 programme package (Frisch et al. 2009). Our results show that $\text{CH}_3\text{C}_4\text{H}$ is the global minimum, while $\text{H}_2\text{CCCHCCH}$ and HCCCH_2CCH lie at 1.44 kJ mol^{-1} and 1.62 kJ mol^{-1} , respectively, over $\text{CH}_3\text{C}_4\text{H}$.

Spectroscopic constants for $\text{H}_2\text{CCCHCCH}$ were derived from a fit to the lines reported by McCarthy et al. (2020) and implemented in the MADEX code (Cernicharo 2012). Nineteen lines with $K_a=0, 1, 2,$ and 3 have been detected in TMC-1. A selected sample of them is shown in Fig. 1. Derived frequencies and line parameters are given in Table A.1. All lines of allenyl acetylene that are not blended with lines from other species and with expected intensities above 1 mK were detected in our survey. Four additional features, with expected intensities of 1-3 mK, fall in the middle of a forest of lines produced by H_2CCN (Cabezas et al. 2021) so that deriving their frequencies and intensities was unreliable.

In order to compute column densities, we calculated the electric dipole moment components of $\text{H}_2\text{CCCHCCH}$ at the MP2/cc-pVTZ level of theory. The $|\mu_a|$ and $|\mu_b|$ derived values are 0.630 D and 0.011 D, respectively. They are in agreement with those previously reported by Lee & McCarthy (2019), which were obtained using a density functional theory level of theory (M05/6-31G(d)).

An analysis of the observed intensities through a rotational diagram provides a rotational temperature of $9 \pm 1 \text{ K}$. We performed a model fitting directly to the observed line profiles as described by Cernicharo et al. (2021a), with the result that the best match between the computed synthetic spectrum and the observations was obtained for $T_r=7 \text{ K}$ and $N(\text{H}_2\text{CCCHCCH})=(1.2 \pm 0.2) \times 10^{13} \text{ cm}^{-2}$. Figure 1 shows the synthetic spectrum. Only the transition $9_{19} - 8_{1,8}$ required a correction intensity by a factor of 0.8, while for all the other lines the model matches the observations perfectly. Using the H_2 column density derived by Cernicharo et al. (1987), the abundance of $\text{H}_2\text{CCCHCCH}$ relative to H_2 towards TMC-1 is 1.2×10^{-9} . This abundance is similar to that of vinyl acetylene (Cernicharo et al. 2021a), about ~ 3 below that of propylene (CH_3CHCH_2 ; Marcelino et al. 2007), and a factor of ten below that of methyl acetylene (CH_3CCH ; Cabezas et al. 2021). Hence, allenyl acetylene is one of the most abundant hydrocarbons in TMC-1, and probably, together with $\text{CH}_3\text{C}_4\text{H}$ (see Sect. 3.2), the most abundant compound containing five carbon atoms. It is interesting to compare the abundance of allenyl acetylene with that of cyano allene (H_2CCCHCN). This species has been recently analysed by Marcelino et al. (2021), resulting in a rotational temperature of $5.5 \pm 0.3 \text{ K}$ and a column density of $(2.7 \pm 0.2) \times 10^{12} \text{ cm}^{-2}$. Consequently, the abundance ratio of $\text{H}_2\text{CCCHCCH}$ over H_2CCCHCN is ~ 4.5 , that is to say the acetylenic derivative of allene is slightly more abundant than the cyanide one. A similar value (~ 1.8) was obtained for the abundance ratio between CH_2CHCCH and CH_2CHCN (Cernicharo et al. 2021a).

² <http://www.iram.fr/IRAMFR/GILDAS>

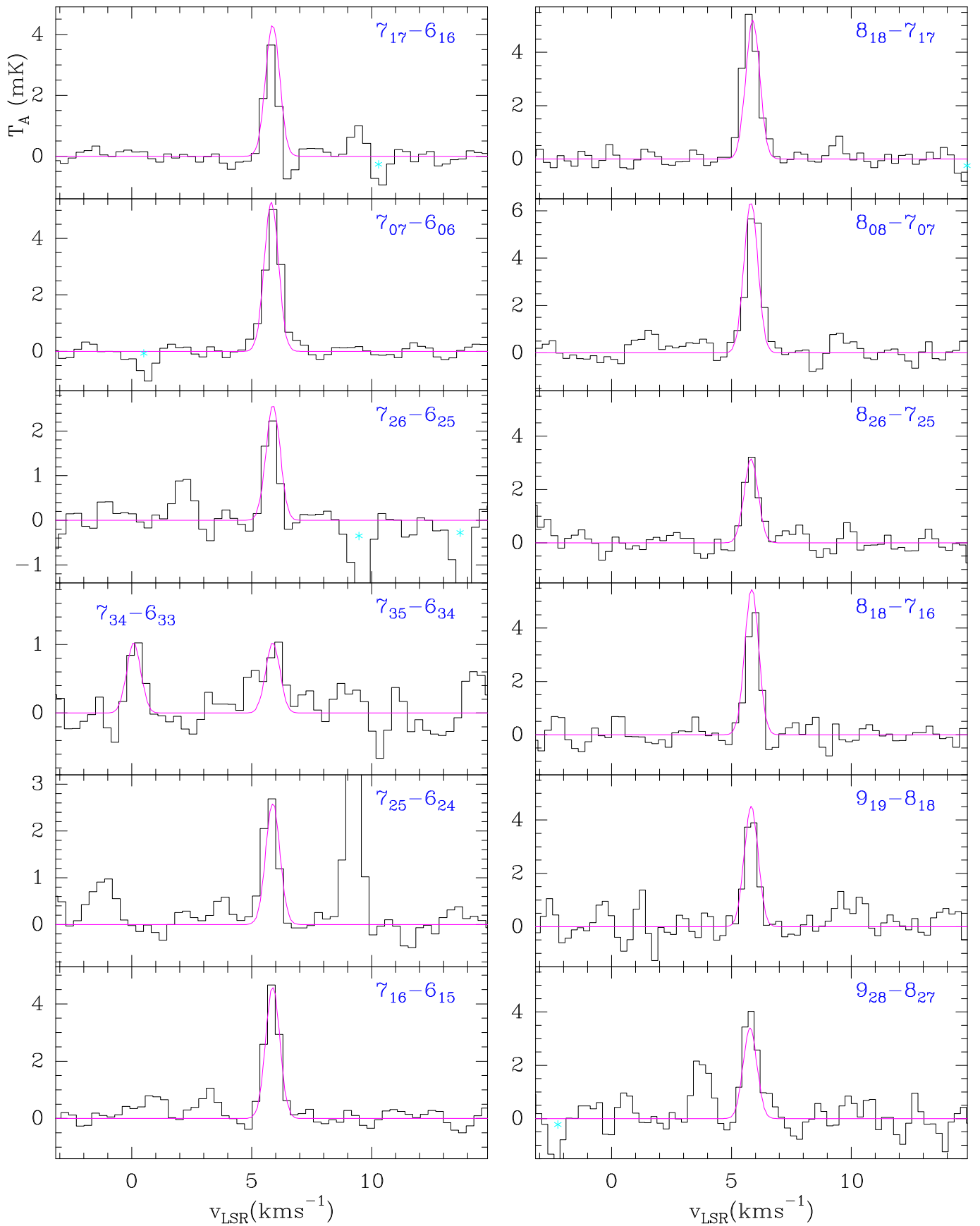


Fig. 1. Observed transitions of H₂CCCHCCH towards TMC-1. The abscissa corresponds to the rest frequency of the lines assuming a local standard of rest velocity of the source of 5.83 km s⁻¹. Frequencies and intensities for the observed lines are given in Table A.1. The ordinate is the antenna temperature, corrected for atmospheric and telescope losses, in millikelvin. The violet line shows the computed synthetic spectrum for this species for $T_r=7$ K and a column density of 1.2×10^{13} cm⁻². Cyan stars indicate the position of negative features produced in the folding of the frequency switching observations.

Table 1. Rotational and distortion constants of H₂CCCHCCH.

Constant	Laboratory ^a	This work
A (MHz)	25963.54(166)	25961.178(785)
B (MHz)	2616.375797(314)	2616.376200(221)
C (MHz)	2412.573364(286)	2412.573306(194)
Δ_J (kHz)	1.15462(391)	1.15734(112)
Δ_{JK} (kHz)	-85.5217(356)	-85.4904(279)
δ_J (kHz)	0.28161(457)	0.28598(132)
Number of lines	14	33
σ (kHz)	1.0	8.5
$J_{max}, K_{a_{max}}$	5, 2	10, 3
ν_{max} (GHz)	25.144	49.218

Notes.

^(a) Laboratory frequencies from McCarthy et al. (2020).

The measured frequencies of the lines observed in TMC-1 can be used to improve the rotational and distortion constants of H₂CCCHCCH. We used the fitting code FITWAT described in Cernicharo et al. (2018). Table 1 provides the results obtained by fitting the laboratory data of McCarthy et al. (2020) alone, and those obtained from a fit to the merged laboratory plus the TMC-1 frequencies. A significant improvement in the uncertainty in the rotational and distortion constants was obtained. The fit to the laboratory data alone results in exactly the same constants as those obtained by McCarthy et al. (2020). The merged fit is recommended to predict the frequency of the rotational transitions of this species above 50 GHz. Predictions could be accurate enough up to 150 GHz to allow for a search of this species in the 3-mm domain. Table B.1 provides the observed and calculated frequencies and their differences.

3.2. Methyl diacetylene, CH₃C₄H

This C₅H₄ isomer was found in TMC-1 by MacLeod et al. (1984) and Walmsley et al. (1984). We used spectroscopic information from Bester et al. (1984), Heath et al. (1955), and Cazoli & Puzzarini (2008) to obtain the rotational constants that were implemented in MADEX (Cernicharo 2012). The dipole moment, 1.207 D, was measured by Bester et al. (1984). The constants A and D_K are taken from Müller et al. (2002). Five rotational transitions, from $J_u = 8$ up $J_u = 12$, lie within our line survey. The $K = 0, 1$, and 2 components of these transitions were observed as shown in Fig. 2. Derived line parameters are given in Table A.2. The detection of the $K=2$ component allows for a good determination of the rotational temperature. As for H₂CCCHCCH, we assumed a uniform brightness source with a radius of 40'' (Fossé et al. 2001). In a first step, we derived T_r from a rotational diagram of the lines of the A and E species. A similar rotation temperature of 7 ± 1 K was obtained for both symmetry species. Then, we produced a synthetic spectrum that was compared with the observed line profiles, allowing us to refine the derived parameters. We found that a synthetic spectrum with $T_r=7$ K and $N(A\text{-CH}_3\text{C}_4\text{H})=N(E\text{-CH}_3\text{C}_4\text{H})=(6.5 \pm 0.2) \times 10^{12} \text{ cm}^{-2}$ matches the observed spectra very well (see Fig. 2). The synthetic spectrum was corrected for beam dilution and beam efficiency. Consequently, the total column density of methyl diacetylene is $(1.3 \pm 0.4) \times 10^{13} \text{ cm}^{-2}$. This value is in good agreement with those derived by Walmsley et al. (1984) and MacLeod et al. (1984) when corrected for the different dipole moment used by these authors (1.0, and 0.9 D, respectively). Hence, both species, allenyl acetylene and methyl diacetylene, have similar abundances in TMC-1. They are only

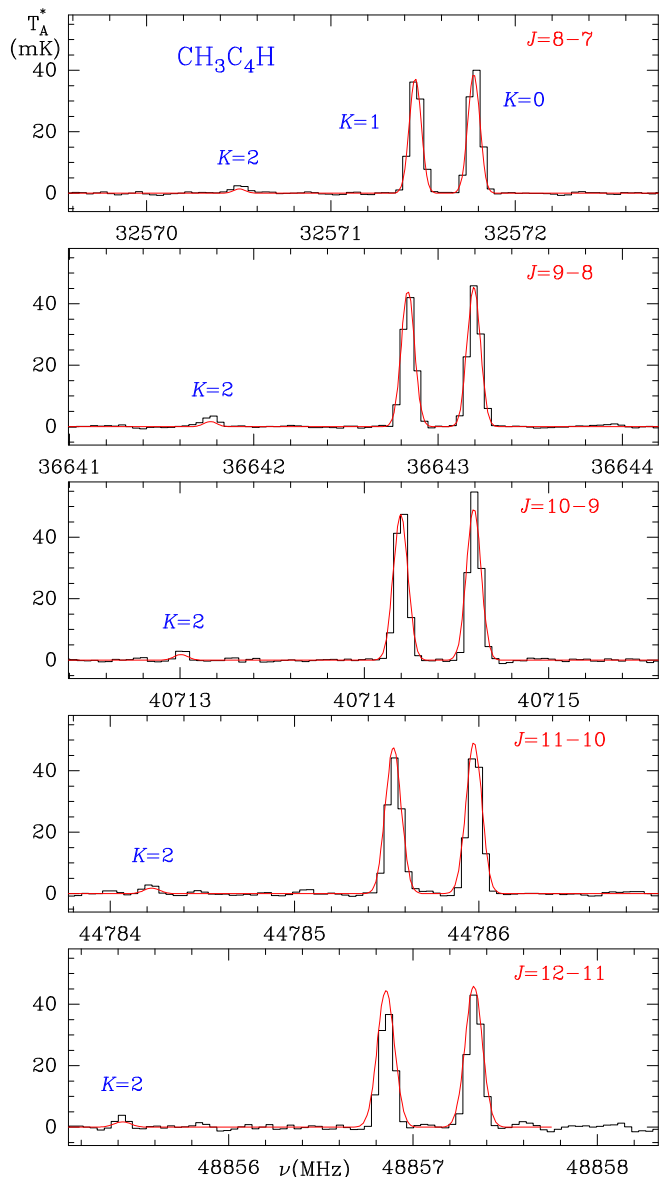


Fig. 2. Observed transitions of CH₃C₄H towards TMC-1. The abscissa corresponds to the rest frequency of the lines assuming a local standard of rest velocity of TMC-1 of 5.83 km s⁻¹. Line parameters for the observed transitions are given in Table A.1. The ordinate is the antenna temperature, corrected for atmospheric and telescope losses, in millikelvin. The red line shows the computed synthetic spectrum for this species for $T_r=7$ K and a column density of $6.5 \times 10^{12} \text{ cm}^{-2}$ for each of the A and E states of vinyl diacetylene.

three times less abundant than propene (Marcelino et al. 2007) and ten times less abundant than methyl acetylene (Cabezas et al. 2021).

3.3. HCCCH₂CCH

We note that 1,4-Pentadiyne, HCCCH₂CCH, is another C₅H₄ isomer. Its rotational spectrum was measured in the laboratory by Kuczkowski et al. (1981). Its dipole moment, 0.52 D, was measured by the same authors. We searched for it through more than ten rotational transitions falling in the 31-50 GHz range. None of them were detected. We derived a 3σ upper limit to its column density of $4 \times 10^{12} \text{ cm}^{-2}$. This moderate upper limit is due to the relatively low dipole moment of this molecule.

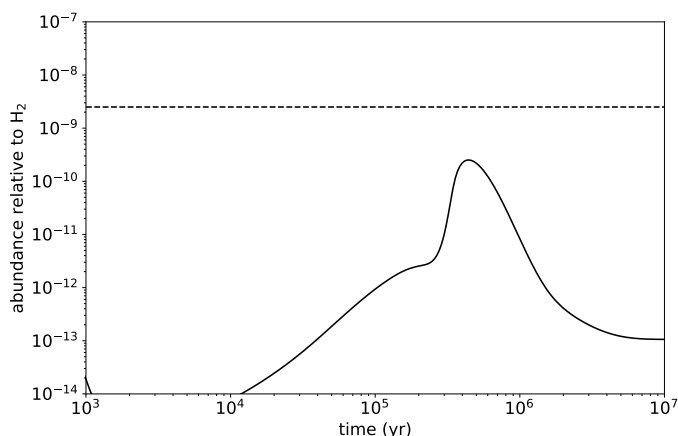
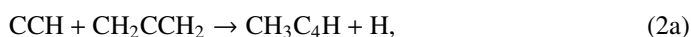


Fig. 3. Calculated fractional abundance of C₅H₄ (allowing for various isomers) as a function of time. The horizontal dashed line corresponds to the sum of the observed abundances of the two C₅H₄ isomers (CH₃C₄H and H₂CCCHCCH) detected in TMC-1.

3.4. Discussion

As a matter of fact, the two most stable C₅H₄ isomers were detected in TMC-1 and both have similar abundances. To learn about the formation of these molecules under cold dark cloud conditions, we carried out chemical model calculations similar to those presented in Marcelino et al. (2021). For chemical model purposes, we considered that the species with molecular formula C₅H₄ accounts for the various possible isomers. According to our chemical model, the peak abundance of C₅H₄ isomers under cold dark cloud conditions is 2.5×10^{-10} relative to H₂, which is ten times smaller than the sum of the observed abundances of CH₃C₄H and H₂CCCHCCH in TMC-1 (see Fig. 3). While the difference between the calculated and observed abundance is significant, it is interesting to inspect which are the main formation routes in the chemical model. Reactions of the CCH radical with methyl acetylene (CH₃CCH) and allene (H₂CCCH₂)



account for most of the C₅H₄ isomers formation. These reactions were experimentally found to be rapid at low temperatures, down to 63 K (Carty et al. 2001), and they are probably also fast at temperatures around 10 K. The reaction of C₂ with propylene, which has also been measured to be rapid down to 77 K (Daugey et al. 2008), is also an important source of C₅H₄ isomers, while a third route involving the dissociative recombination of the ion C₅H₅⁺ does also contribute to their formation.

Although the branching ratios of reactions (1) and (2) are not precisely known, methyl acetylene and allenyl acetylene are the most likely products (Kaiser et al. 2001; Zhang et al. 2009; Goulay et al. 2011). In fact, it would be interesting to verify if CH₃C₄H is the preferred product of reaction (1) and if H₂CCCHCCH is preferentially formed in reaction (2); this would allow one to probe the abundance of the non-polar hydrocarbon allene, which is expected to be large. The chemical scheme depicted by reactions (1) and (2) is similar to that driving the formation of C₄H₃N isomers in which reactions of the CN

radical with CH₃CCH and H₂CCCH₂ are at the heart of the synthesis of the various C₄H₃N isomers, as discussed by Marcelino et al. (2021). In fact, it is worth noting that the abundance ratio C₅H₄/C₄H₃N of 3.5 (Marcelino et al. 2021 and this study) observed in TMC-1 is not far from the CCH/CN abundance ratio of 10 observed in this source (Pratap et al. 1997).

Acknowledgements. We thank Ministerio de Ciencia e Innovación of Spain (MICIU) for funding support through projects AYA2016-75066-C2-1-P, PID2019-106110GB-I00, PID2019-107115GB-C21 / AEI / 10.13039/501100011033, and PID2019-106235GB-I00. We also thank ERC for funding through grant ERC-2013-Syg-610256-NANOCOSMOS. M.A. thanks MICIU for grant RyC-2014-16277.

References

- Agúndez, M. & Wakelam, V. 2013, *Chem. Rev.* 113, 8710
 Bester, M., Yamada, K., Winnewisser, G., et al. 1984, *A&A*, 137, L20
 Cabezas, C., Endo, Y., Roueff, E., et al. 2021, *A&A*, 646, L1
 Carty, D., Le Page, V., Sims, I. R., & Smith, I. W. M. 2001, *Chem. Phys. Lett.*, 344, 310
 Cazzoli, G. & Puzzarini, C. 2008, *A&A*, 487, 1197
 Cernicharo, J. 1985, Internal IRAM report (Granada: IRAM)
 Cernicharo, J., Guélin, M., Hein, H., Kahane, C., 1987, *A&A*, 181, L9
 Cernicharo, J. & Guélin, M. 1996, *A&A*, 309, L27
 Cernicharo, J., 2012, in *ECLA 2011: Proc. of the European Conference on Laboratory Astrophysics*, EAS Publications Series, 2012, Ed.: C. Stehl, C. Joblin, & L. d'Hendecourt (Cambridge: Cambridge Univ. Press), 251; https://nanocosmos.iff.csic.es/?page_id=1619
 Cernicharo, J., Kisiel, Z., Tercero, B., et al. 2016, *A&A*, 587, L4
 Cernicharo, J., Guélin, M., Agúndez, M., et al. 2018, *A&A*, 618, A4
 Cernicharo, J., Cabezas, C., Pardo, J. R., et al. 2019, *A&A*, 630, L2
 Cernicharo, J., Marcelino, N., Agúndez, M., et al. 2020a, *A&A*, 642, L17
 Cernicharo, J., Marcelino, N., Pardo, J.R., et al. 2020b, *A&A*, 641, L9
 Cernicharo, J., Marcelino, N., Agúndez, M., et al. 2020c, *A&A*, 642, L8
 Cernicharo, J., Agúndez, M., Cabezas, C., et al. 2021a, *A&A*, submitted
 Cernicharo, J., Cabezas, C., Bailleux, S., et al. 2021b, *A&A*, in press, 2021arXiv210104603C
 Cernicharo, J., Cabezas, C., Endo, Y., et al. 2021c, *A&A*, in press, 2021arXiv210105163C
 Daugey, N., Caubet, P., Bergeat, A., et al. 2008, *PCCP*, 10, 729
 Dunning, T. H., 1989, *J. Chem. Phys.* 90, 1007
 Fossé, D., Cernicharo, J., Gerin, M., Cox, P. 2001, *ApJ*, 552, 168
 Frisch, M. J., Trucks, G. W., Schlegel, H. B., et al. 2009, *Gaussian 09*, revision D.01
 Goulay, F., Soorkia, S., Meloni, G., et al. 2011, *PCCP*, 13, 20820
 Heath, G.A., Thomas, L.F., Sherrard, E.I., et al. 1955, *Discussions Farad. Soc.*, 19, 38
 Kaifu, N., Ohishi, M., Kawaguchi, K., et al. 2004, *PASJ*, 56, 69
 Kaiser, R. I., Chiong, C. C., Asvany, O., et al. 2001, *J. Chem. Phys.*, 114, 3488
 Kawaguchi, K., Fujimori, R. & Sayaka, A. 2007, *PASJ*, 59, L47
 Krańnicki, A. & Kisiel, Z. 2011, *J. Mol. Spectrosc.*, 270, 83
 Kuzckowski, R.L., Lovas, F.L., Suenram, R.D., et al. 1981, *J. Mol. Struct.*, 72, 143
 Lee, K. L. K. & McCarthy, M., 2019, *J. Phys. Chem. Lett.*, 10, 2408
 Lide Jr, D.R. & Mann, D.E. 1957, *J. Chem. Phys.*, 27, 868
 MacLeod, J.M., Avery, L.W., Broten, N.W. 1984, *ApJ*, 282, L89
 Marcelino, N., Cernicharo, J., & Agúndez, M. 2007, *ApJ*, 665, L127
 Marcelino, N., Agúndez, M., Tercero, B., et al. 2020, *A&A*, 643, L6
 Marcelino, N., Tercero, B., Agúndez, M., & Cernicharo, J. 2021, *A&A*, in press, arxiv.org/abs/2101.08516
 McCarthy, M.C., et al., 2020, *J. Phys. Chem. A*, 124, 5170
 Møller, C., & Plesset, M. S., 1934, *Phys. Rev.* 46, 618
 Müller, H. S. P., Pracna, P. & Horneman, V. -M. 2002, *J. Mol. Spectrosc.*, 216, 397
 Müller, H.S.P., Schlöder, F., Stutzki, J., Winnewisser, G. 2005, *J. Mol. Struct.*, 742, 215
 Ozier, I., Ho, W., & Birnbaum, G. 1969, *J. Chem. Phys.*, 51, 4873
 Pardo, J. R., Cernicharo, J., Serabyn, E. 2001, *IEEE Trans. Antennas and Propagation*, 49, 12
 Pickett, H.M., Poynter, R. L., Cohen, E. A., et al. 1998, *J. Quant. Spectrosc. Radiat. Transfer*, 60, 883
 Pratap, P., Dickens, J. E., Snell, R. L., et al. 1997, *ApJ*, 486, 862
 Remijan, A.J., Hollis, J.M. & Lovas, F.J. 2007, *ApJ*, 664, L47
 Sakai, N., Shirley, Y., Sakai, T., et al., 2012, *ApJ*, 758, L4
 Sobolev, G.A., Shcherbakov, A.M., & Akishin, P.A. 1962, *Opt. Spectrosc.*, 12, Tercero, F., López-Pérez, J. A., Gallego, et al. 2021, *A&A*, 645, A37
 Walmsley, C.M., Jewell, P.R., Snyder, L.E. & Winnewisser, G. 1984, *A&A*, 184, L11
 Zhang, F., Kim, S., & Kaiser, R. I. 2009, *PCCP*, 11, 4707

Table A.1. Observed line parameters for CH₂CCHCCH in TMC-1.

JK_aK_c	ν_{obs}^a (MHz)	$\int T_A^* dv^b$ (mK km s ⁻¹)	Δv^c (km s ⁻¹)	T_A^* (mK)
7 _{1,7} – 6 _{1,6}	34472.262(10)	2.4±0.4	0.60±0.05	3.7±0.3 ^d
7 _{0,7} – 6 _{0,6}	35126.923(10)	4.0±0.5	0.77±0.05	4.8±0.3
7 _{2,6} – 6 _{2,5}	35195.532(10)	1.6±0.4	0.63±0.07	2.4±0.3
7 _{3,5} – 6 _{3,4}	35222.531(10)	1.0±0.4	0.70±0.20	1.3±0.3
7 _{3,4} – 6 _{3,3}	35223.195(10)	0.7±0.3	0.60±0.17	1.0±0.3
7 _{2,5} – 6 _{2,4}	35269.664(10)	2.2±0.5	0.74±0.08	2.7±0.3
7 _{1,6} – 6 _{1,5}	35897.418(10)	3.6±0.5	0.73±0.05	4.7±0.3
8 _{1,8} – 7 _{1,7}	39390.116(10)	4.3±0.4	0.77±0.04	5.3±0.3
8 _{0,8} – 7 _{0,7}	40118.252(10)	4.7±0.4	0.72±0.05	6.1±0.3
8 _{2,7} – 7 _{2,6}	40218.511(20)	0.8±0.4	0.50±0.20	1.6±0.3 ^e
8 _{2,6} – 7 _{2,5}	40329.448(10)	2.6±0.6	0.75±0.09	3.2±0.4
8 _{1,7} – 7 _{1,6}	41018.002(10)	2.7±0.5	0.55±0.06	4.6±0.4
9 _{1,9} – 8 _{1,8}	44305.369(10)	2.8±0.5	0.61±0.07	4.3±0.5
9 _{0,9} – 8 _{0,8}	45099.094(20)	4.4±1.0	0.57±0.02	8.0±2.0 ^f
9 _{2,8} – 8 _{2,7}	45239.452(10)	3.2±0.8	0.73±0.10	4.1±0.6
9 _{3,7} – 8 _{3,6}	45291.918(10)			^g
9 _{3,6} – 8 _{3,5}	45294.382(20)	1.3±0.5	0.69±0.17	1.9±0.5
9 _{2,7} – 8 _{2,6}	45397.522(20)	1.5±0.5	0.52±0.15	1.8±0.6 ^h
9 _{1,8} – 8 _{1,7}	46135.431(10)	2.3±0.5	0.60±0.07	4.7±0.6
10 _{1,10} – 9 _{1,9}	49217.784(10)	3.2±0.7	0.65±0.10	4.9±0.6

Notes.

- (^a) Observed frequency assuming a v_{LSR} of 5.83 km s⁻¹.
(^b) Integrated line intensity in mK km s⁻¹.
(^c) Linewidth at half intensity derived by fitting a Gaussian function to the observed line profile (in km s⁻¹).
(^d) Blended with a negative feature produced in the folding of the frequency switching observing procedure.
(^e) Blended with two negative features produced in the frequency switching folding. The intensity is uncertain
(^f) Heavily blended with HCCCH₂CN. Frequency difference between both lines lower than 20 kHz. We estimate that the contribution of this contaminating feature, by comparison with other similar lines of this species, is ~50%
(^g) Fully blended with a negative feature produced in the frequency switching folding. The fit is unreliable.
(^h) Blended with two lines from other species. The separation between them still allows for a reasonable fit to the line parameters.

Appendix A: Line parameters of H₂CCHCCH and CH₃C₄H

Line parameters for the different molecules studied in this work were obtained by fitting a Gaussian line profile to the observed data. A window of ± 20 km s⁻¹ around the v_{LSR} of the source was considered for each transition. The derived line parameters for H₂CCCHCCH are given in Table A.1. Those of CH₃C₄H are provided in Table A.2.

Appendix B: Observed and calculated frequencies for H₂CCHCCH

In this section, we provide the full list of observed and calculated frequencies for allyl cyanide. The laboratory data come from McCarthy et al. (2020). All lines were weighted in the fit as $1/\sigma^2$. Laboratory data have an accuracy of 2 kHz, while the corresponding uncertainty for the rotational transitions measured in TMC-1 is 10 kHz, with the exception of four lines showing some partial blending with other features for which we assigned an uncertainty of 20 kHz.

Table A.2. Observed line parameters for CH₃C₄H in TMC-1.

J_u	K	ν (MHz)	$\int T_A^* dv^a$ (mK km s ⁻¹)	v_{LSR}^b (km s ⁻¹)	Δv^c (km s ⁻¹)	T_A^* ^d (mK)
8	2	32570.504	2.1 ± 0.5	5.80 ± 0.05	0.82 ± 0.11	2.4 ± 0.3
8	1	32571.457	30.8 ± 0.7	5.80 ± 0.02	0.74 ± 0.01	39.3 ± 0.3
8	0	32571.775	33.6 ± 0.7	5.80 ± 0.02	0.73 ± 0.01	42.8 ± 0.3
9	2	36641.764	2.8 ± 0.5	5.81 ± 0.03	0.79 ± 0.07	3.4 ± 0.3
9	1	36642.836	32.0 ± 0.7	5.79 ± 0.04	0.69 ± 0.01	43.8 ± 0.3
9	0	36643.194	33.9 ± 0.7	5.80 ± 0.02	0.69 ± 0.01	46.3 ± 0.3
10	2	40713.005	2.0 ± 0.5	5.78 ± 0.03	0.47 ± 0.08	3.9 ± 0.4
10	1	40714.197	31.9 ± 0.7	5.81 ± 0.02	0.57 ± 0.01	53.0 ± 0.4
10	0	40714.594	34.2 ± 0.7	5.80 ± 0.02	0.58 ± 0.01	55.2 ± 0.4
11	2	44784.226	2.2 ± 0.7	5.89 ± 0.05	0.61 ± 0.10	3.4 ± 0.5
11	1	44785.536	30.0 ± 0.8	5.79 ± 0.02	0.63 ± 0.01	44.5 ± 0.5
11	0	44785.973	30.9 ± 0.8	5.80 ± 0.02	0.60 ± 0.02	48.6 ± 0.5
12	2	48855.424	1.9 ± 0.6	5.85 ± 0.04	0.44 ± 0.07	4.1 ± 0.6
12	1	48856.853	23.8 ± 0.8	5.80 ± 0.02	0.57 ± 0.01	39.1 ± 0.6
12	0	48857.330	27.1 ± 0.8	5.80 ± 0.02	0.58 ± 0.01	44.2 ± 0.6

Notes. (^a) Observed frequency assuming a v_{LSR} of 5.83 km s⁻¹.

(^b) Local standard of rest velocity of the line in km s⁻¹.

(^c) Integrated line intensity in mK km s⁻¹.

(^d) Linewidth at half intensity derived by fitting a Gaussian function to the observed line profile (in km s⁻¹).

Table B.1. Observed frequencies for H₂CCCHCCH in the laboratory and in TMC-1.

Transition	ν (MHz)	Unc. (MHz)	ν_{cal} (MHz)	Unc. (MHz)	$\nu(obs - cal)$ (MHz)	
2 _{1,2} – 1 _{1,1}	9854.409	0.002	9854.4102	0.0004	-0.0012	A
2 _{0,2} – 1 _{0,1}	10056.532	0.002	10056.5335	0.0003	-0.0015	A
2 _{1,1} – 1 _{1,0}	10261.996	0.002	10261.9977	0.0005	-0.0017	A
3 _{1,3} – 2 _{1,2}	14780.736	0.002	14780.7355	0.0006	0.0005	A
3 _{0,3} – 2 _{0,2}	15081.411	0.002	15081.4106	0.0004	0.0004	A
3 _{2,2} – 2 _{2,1}	15088.775	0.002	15088.7753	0.0005	-0.0003	A
3 _{1,2} – 2 _{1,1}	15392.077	0.002	15392.0770	0.0007	0.0000	A
4 _{1,4} – 3 _{1,3}	19706.013	0.002	19706.0129	0.0007	0.0001	A
4 _{0,4} – 3 _{0,3}	20102.224	0.002	20102.2239	0.0006	0.0001	A
4 _{2,3} – 3 _{2,2}	20117.206	0.002	20117.2044	0.0006	0.0016	A
4 _{2,2} – 3 _{2,1}	20130.481	0.002	20130.4822	0.0006	-0.0012	A
4 _{1,3} – 3 _{1,2}	20521.046	0.002	20521.0456	0.0008	0.0004	A
5 _{1,5} – 4 _{1,4}	24629.906	0.002	24629.9066	0.0007	-0.0006	A
5 _{2,4} – 4 _{2,3}	25144.638	0.002	25144.6375	0.0007	0.0005	A
7 _{1,7} – 6 _{1,6}	34472.262	0.010	34472.2569	0.0013	0.0051	B
7 _{0,7} – 6 _{0,6}	35126.923	0.010	35126.9230	0.0020	0.0000	B
7 _{2,6} – 6 _{2,5}	35195.532	0.010	35195.5240	0.0011	0.0080	B
7 _{3,5} – 6 _{3,4}	35222.531	0.010	35222.5236	0.0025	0.0074	B
7 _{3,4} – 6 _{3,3}	35223.195	0.010	35223.2044	0.0024	-0.0094	B
7 _{2,5} – 6 _{2,4}	35269.664	0.010	35269.6575	0.0024	0.0065	B
7 _{1,6} – 6 _{1,5}	35897.418	0.010	35897.4116	0.0019	0.0064	B
8 _{1,8} – 7 _{1,7}	39390.116	0.010	39390.1081	0.0021	0.0079	B
8 _{0,8} – 7 _{0,7}	40118.252	0.010	40118.2535	0.0030	-0.0015	B
8 _{2,7} – 7 _{2,6}	40218.511	0.020	40218.4833	0.0016	0.0277	B
8 _{2,6} – 7 _{2,5}	40329.448	0.010	40329.4495	0.0038	-0.0015	B
8 _{1,7} – 7 _{1,6}	41018.002	0.010	41017.9994	0.0029	0.0026	B
9 _{1,9} – 8 _{1,8}	44305.369	0.010	44305.3697	0.0031	-0.0007	B
9 _{0,9} – 8 _{0,8}	45099.094	0.020	45099.0983	0.0044	-0.0043	B
9 _{2,8} – 8 _{2,7}	45239.452	0.010	45239.4588	0.0023	-0.0068	B
9 _{3,6} – 8 _{3,5}	45294.382	0.020	45294.4077	0.0034	-0.0257	B
9 _{2,7} – 8 _{2,6}	45397.522	0.020	45397.5168	0.0055	0.0052	B
9 _{1,8} – 8 _{1,7}	46135.431	0.010	46135.4358	0.0043	-0.0048	B
10 _{1,10} – 9 _{1,9}	49217.784	0.010	49217.7869	0.0045	-0.0029	B

Notes.^(A) Observed frequencies in the laboratory are from McCarthy et al. (2020).^(B) Frequencies observed in TMC-1 adopting a v_{LSR} of 5.83 km s⁻¹.^(b) Observed minus calculated frequencies in MHz.